



## Chemical Solution Deposition of Ferroelectric Hafnium Oxide for Future Lead Free Ferroelectric Devices

Sergej Starschich, David Griesche, Theodor Schneller, and Ulrich Böttger<sup>z</sup>

Institut für Werkstoffe der Elektrotechnik 2, RWTH Aachen University, D-52074 Aachen, Germany

The phase formation and the influence of the type of dopant of an improved routine for chemical solution deposition (CSD) of ferroelectric hafnium oxide films are investigated. Ferroelectric properties for yttrium doping and doping with different elements from the lanthanide group are shown. The samples are prepared using platinum electrodes and a hafnium oxide layer with a thickness of 45 nm. The combination of DTA-TG analysis, thickness measurements and temperature dependent XRD study provide insight into the film formation process during the different fabrication steps. Polarization and capacitance measurements are performed to prove the ferroelectric nature of the deposited layers. The yttrium concentration is varied in a range from 0 mol% to 11 mol% proving to have a strong influence on the ferroelectric properties in agreement with the observation made on atomic layer deposition (ALD) prepared samples. A high remanent polarization of  $20 \mu\text{C cm}^{-2}$  is attained with a coercitive field of  $1.4 \text{ MV cm}^{-1}$  for an yttrium doping concentration of 5.2 mol%. The possibility of depositing ferroelectric hafnium oxide films by CSD provides the opportunity of application for lead free piezoelectric and pyroelectric sensors and actuators and can lead to a better insight into the formation of the ferroelectric phase.

© 2015 The Electrochemical Society. [DOI: [10.1149/2.0061512jss](https://doi.org/10.1149/2.0061512jss)] All rights reserved.

Manuscript submitted August 7, 2015; revised manuscript received September 8, 2015. Published September 16, 2015.

Recently an unconventional lead free ferroelectric thin film material, based on doped hafnium oxide has been discovered.<sup>1</sup> In contrast to the conventional, mostly lead based ferroelectrics, hafnium oxide is completely compatible with known semiconductor fabrication processes. In the information technology, hafnium oxide based ferroelectric memories are promising candidates for future high density, nonvolatile devices.<sup>2</sup> Due to the fact that every ferroelectric material also exhibit piezoelectric and pyroelectric properties, further fields of applications are piezoelectric and pyroelectric sensors and actuators. In particular, the area of pyroelectric energy harvesting and storage is of great interest.<sup>3-8</sup> In spite of considerable effort, the physical origin of the stabilization of the ferroelectric phase in these films is not well understood yet. The ferroelectricity is attributed to the non-centrosymmetric orthorhombic phase with a  $\text{Pbc}2_1$  space group.<sup>1</sup> Up to now almost all ferroelectric hafnium oxide thin films have been prepared by gas phase methods such as sputtering, metal-organic chemical vapor deposition (MOCVD) or ALD. In all of these studies ferroelectricity was shown for ultrathin films of approximately 10 nm and reduction of the remanent polarization for thicker films was observed for ALD samples by Park et al. Only recently, it could be shown by the fabrication of thicker films by CSD that ferroelectricity in this material is not directly related to the very thin film thickness.<sup>10</sup>

The possibility of using CSD for the layer preparation moreover provides the opportunity of inexpensive and flexible device preparation for future lead free sensors and actuators. Furthermore, due to the relative ease of CSD solution preparation the influence of the doping elements can be studied extensively and may lead to a better comprehension about the origin of the ferroelectric phase. The ferroelectricity of hafnium oxide samples prepared by ALD was shown for several dopants.<sup>1,11-15</sup>

In this work an optimized CSD routine compared to a recent publication is presented.<sup>10</sup> For this purpose, the hafnium tetra ethoxide has been replaced by hafnium tetra acetyl acetonate, which avoids the stabilization step during synthesis. An additional heating step after each spin coating leads to better ferroelectric properties after the crystallization. The CSD process is investigated in greater depth regarding solution properties, layer deposition and phase formation. Furthermore, ferroelectricity is shown for doping with different elements from the lanthanide group. The yttrium doped layers show similar behavior to the samples prepared by ALD concerning the characteristic ferroelectric properties and the dependence on the doping concentration.<sup>13</sup>

### Experimental

For the preparation of the precursor solutions, a metallo-organic decomposition (MOD) routine was applied.<sup>16</sup> The desired amount of Hafnium 2,4-pentandionate (Alfa Aesar) and the 2,4-pentandionate of the corresponding doping metal (Alfa Aesar) was weighted into a Schlenk flask in a glove box with inert gas atmosphere. Subsequently the two educts were dissolved in a mixture (5:1) of propionic acid (Merck, f.s.) and propionic acid anhydride (Merck, f.s.) at  $130^\circ\text{C}$ . By adding propionic acid, a concentration of 0.25 mol/l was adjusted. The prepared yellow precursor solution was spin coated on a  $1 \text{ cm}^2$  substrate covered with a 100 nm thick planar platinum bottom electrode. After each spin coating, a heating step at varying temperatures between  $215^\circ\text{C}$  and  $295^\circ\text{C}$  was performed in ambient atmosphere for five minutes. To achieve a resulting thickness of 45 nm, three coatings were carried out. The crystallization was realized in a RTP (Rapid Thermal Processing) step at  $800^\circ\text{C}$  for 90 seconds in an argon/oxygen (1:1) atmosphere showing the best electrical results. Afterwards the patterned 50 nm platinum top electrodes were deposited at room temperature by a negative lift-off process. The different steps during the preparation procedure are shown in Figure 1.

The polarization (P-V) measurements were carried out using an aixACCT Systems TF Analyzer 2000. A HP4284A LCR meter was used to record the capacitance measurements (C-V), whereas PANalytical XPert Pro was used for the Grazing Incidence X-Ray Diffractions (GI-XRD) and X-Ray Reflectivity (XRR) thickness measurements. Temperature dependent GI-XRD Measurements were realized with a self-built temperature stage. The DTA-TG analysis was carried out with a Mettler Toledo 851a at a heating ramp of  $5^\circ\text{C/min}$ . To prepare for the analysis the solution was dried in a round bottom flask by means of a heating mantle until all volatile constituents were removed. An amount of 23.3 mg precursor powder with  $\text{Al}_2\text{O}_3$  as the reference was used for the analysis. The P-V and C-V curves were measured at a frequency of 1 kHz with a 50 mV ac probing signal for the C-V measurements on device areas of  $2.5 \times 10^{-4} \text{ cm}^2$ . As reported in,<sup>10</sup> a certain amount of “wake-up” cycles is necessary to exhibit ferroelectric properties. For all electrical data shown here 1000 cycles were performed beforehand at a voltage of 13 V.

### Results and Discussion

In order to figure out temperature ranges suitable for pyrolysis and crystallization of the as-deposited films, differential thermoanalysis coupled with thermogravimetry (DTA-TG) has been performed exemplarily from the dry precursor powder of 5.2% Y doped  $\text{HfO}_2$  in air. The corresponding DTA-TG results are shown in Figure 2. At first, the vaporization of small amounts of residual solvent ( $\sim 1\%$ ) occurs

<sup>z</sup>E-mail: [boettger@iwe.rwth-aachen.de](mailto:boettger@iwe.rwth-aachen.de)

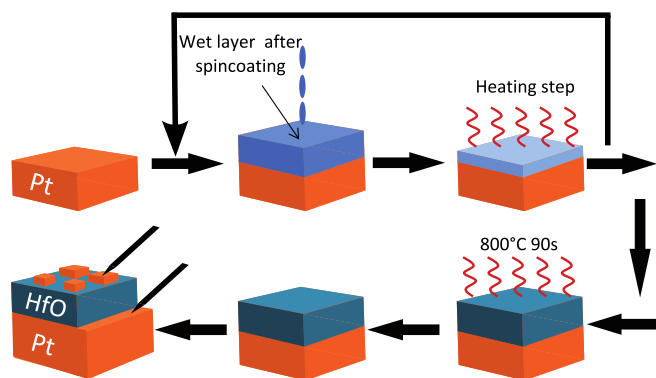


**Figure 1.** Workflow for the sample preparation: The solution is deposited on the platinum substrate and afterwards heated at varying temperatures for five minutes on a hot plate. These two steps are repeated three times to achieve the aimed thickness of 45 nm. Afterwards a crystallization step at 800°C is performed for 90 seconds in a RTA oven. Finally the top electrodes are deposited by a negative lift off process.

at lower temperatures i.e. below  $\sim 160^\circ\text{C}$ , which is indicated by the endothermic peaks in the DTA curve. This is followed by a further continuous weight loss which merges into the range of the exothermic decomposition of the metallo-organic precursors molecules. This pyrolysis starts at approx.  $250^\circ\text{C}$  and reaches its maximum at  $415^\circ\text{C}$  indicated by the exothermic peak of the DTA signal. At  $\sim 490^\circ\text{C}$  the pyrolysis is completed and no further weight loss is observed for higher temperatures. In this phase of the thermal transformation process the largest weight loss of approx. 40% is observed. Assuming that the yttrium and hafnium acetyl acetonate compounds are solely dissolved during the solution preparation, the overall weight loss during pyrolysis should be 63.6% which is significantly higher than the 40% observed in the DTA analysis (Figure 2). In order to explain this discrepancy a chemical reaction of the initial metal acetyl acetonato complexes and the propionic acid used as a solvent during solution synthesis has to be taken into account. Further evidence that chemical bonds are formed during solution preparation is that pure yttrium acetyl acetonate does not solve permanently in propionic acid/propionic acid anhydride but in combination with the hafnium acetyl acetonate it dissolves well. Similar observations have been reported in the literature for zirconium acetylacetone based precursor

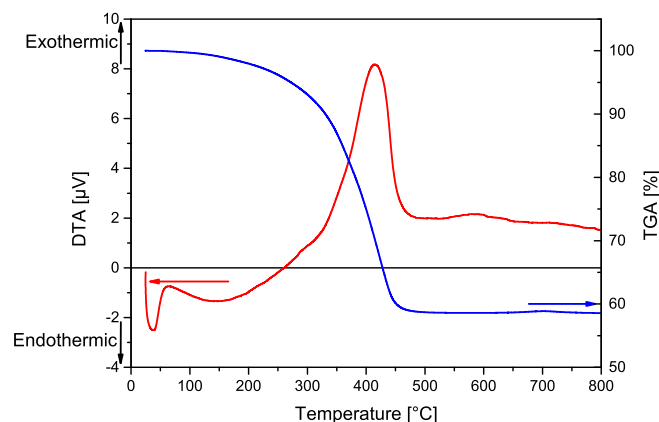


**Figure 2.** DTA TG analysis of the dried precursor with 5.2% yttrium doping at a heating rate of  $5^\circ\text{C}/\text{min}$  in ambient atmosphere. For temperatures above  $\sim 250^\circ\text{C}$  the exothermic pyrolysis sets in and reaches its maximum at approximately  $415^\circ\text{C}$ . During the pyrolysis the mass of the precursor powder is reduced by  $\sim 40\%$  due to the evaporation of the combustion products until the relative mass of the pure amorphous metal oxides is reached. An exothermic hump at approx.  $586^\circ\text{C}$  indicates the transition of the amorphous metal oxides to the crystalline material.

solutions.<sup>17–19</sup> Since hafnium and zirconium show nearly identical chemical behavior it is concluded that a reaction with propionic acid took place here as well. However a simple complete ligand substitution by propionate groups can be ruled out because the expected mass loss of 55.4% is significantly higher as the observed loss (40%). Most probably a more complex Hf cluster structure containing bridging oxo groups and carboxylate groups has been formed, similar to what has been found in case of the reaction of  $\text{Zr}(\text{acac})_4$  with propionic acid.<sup>17</sup> Moreover it is assumed that the yttrium compound is linked to this hafnium cluster, e.g. via a carboxylate group. The fact that yttrium acetyl acetonate only dissolves well in propionic acid in the presence of the Hf-cluster points to this opportunity but the exact structure of the precursor molecule is not known yet and its determination is beyond the scope of this work. The small exothermic hump above  $550^\circ\text{C}$  with its maximum at  $\sim 586^\circ\text{C}$  probably indicates the crystallization of the powder. Figure 3 shows the evolution of the film thickness of one single coating step in dependence of the applied process temperatures and models of the corresponding assumed layer structure during each step with the corresponding XRR measurements. Figure 3a shows schematically the wet, as-deposited layer after spin coating with the corresponding thickness measured by XRR. It is obvious that this film contains the metallo-organic hafnium precursor clusters distributed in a considerable amount of propionic acid. By application of the relative low temperature of  $215^\circ\text{C}$  during the first heating step the film starts to densify accompanied with the reduction of the film thickness (Figure 3b). Based on the thermal analysis we assume that predominantly vaporization of the solvent occurs and almost no pyrolytic decomposition takes place (Figure 3b). If higher temperatures are applied at this stage, lower film thicknesses (inset of Figure 3) are obtained accompanied with a higher degree of pyrolytic decomposition. In order to induce crystallization the second heat-treatment step was performed by an RTA oven at  $800^\circ\text{C}$ . During this process the main part of pyrolysis and finally crystallization inextricably takes place leading to an organic free yttrium doped hafnium oxide layer (Figure 3c).

In order to investigate the influence of different temperatures of the first heat-treatment step on the ferroelectric properties, a series of hot plate temperatures between  $180^\circ\text{C}$  and  $295^\circ\text{C}$  was applied to thin film samples. It turned out that the lowest applicable temperature for the multi-coating process which is necessary to get a film thickness suitable for ferroelectric characterization (i.e. 45 nm) is  $215^\circ\text{C}$ . Note, if the first layer is heated below this temperature it is simply dissolved by the subsequent spin-on process and no increase of the film thickness could be obtained.

Interestingly the electrical properties change considerably for the different temperatures applied in the first step as shown in Figure 4 for the permittivity and the ferroelectric hysteresis. The best ferroelectric properties result from films which have been rather dried at  $215^\circ\text{C}$  than pyrolyzed. By applying a temperature of  $295^\circ\text{C}$  the remanent polarization is reduced by 40% compared to the heat-treatment at  $215^\circ\text{C}$ . A possible explanation is that the presence of the organic part prevents the growth of larger inhomogeneously composed cluster units. This in turn might help to maintain a solution like homogeneity of the metallo-organic precursors in the dried or only partially pyrolyzed films up to higher temperatures where sufficient energy is available for the crystallization process. Thus more homogeneously composed ferroelectric films with superior properties result as shown in Figure 4. For the further shown results a first heat-treatment temperature of  $215^\circ\text{C}$  is used. Figure 5 shows the influence of the crystallization temperature on the electrical properties and crystal structure. A cubic structure can be observed at  $600^\circ\text{C}$ . The corresponding hysteresis shows a high leakage current indicated by the strong split up of the hysteresis at higher voltages. This can probably be explained by remains of organic parts in the layer. For  $700^\circ\text{C}$  the leakage current is strongly reduced and a hysteresis with a remanent polarization of approximately  $10 \mu\text{C}/\text{cm}^2$  is measured. At  $800^\circ\text{C}$  the best electrical results can be observed. The XRD results show the highest orthorhombic fraction is given at  $900^\circ\text{C}$  but no electrical results are given for this temperature due to break down of the devices during wake-up. Figure 6a) shows the influence of the yttrium concentration on the ferroelectric hysteresis

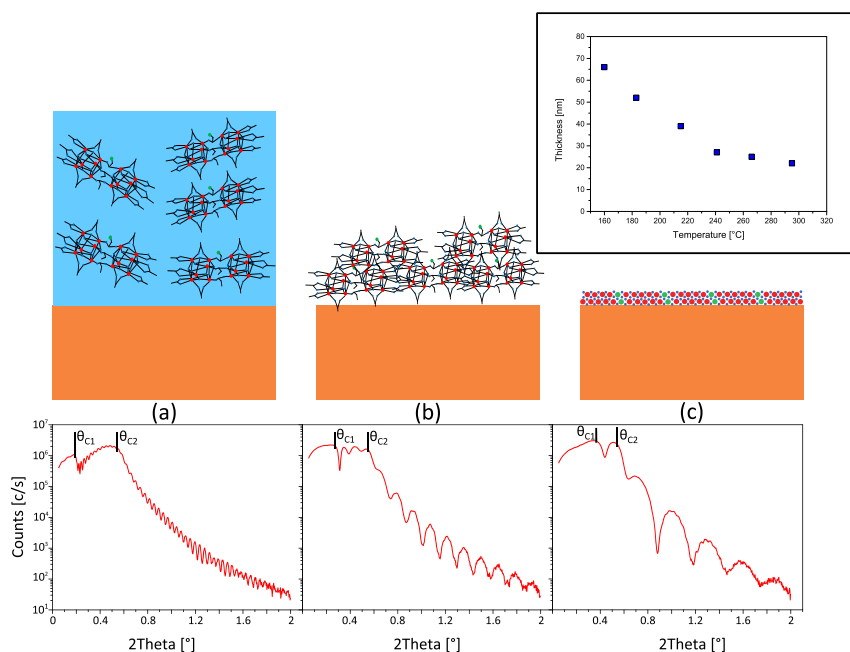


**Figure 3.** Influence of the two different heating steps on the deposited layer. The three sketches in the upper part of the figure show schematically the assumed layer structure for the different conditions. Below each sketch the corresponding XRR measurements are displayed.  $\theta_{c1}$  is the critical angle of the deposited layer indicating the surface density and  $\theta_{c2}$  is the critical angle of the platinum substrate which is constant for all conditions. (a): Directly after spin coating, the hafnium clusters are distributed in the wet, as-deposited layer which has a thickness of 114 nm. (b): Situation after the first heating step, exemplarily shown for a temperature of 215°C. During the heat-treatment at this temperature only the propionic acid is vaporized and a layer thickness of 38 nm remains. (c): After the crystallization at 800°C a layer thickness of 15 nm is measured with a higher density compared to (a) and (b) indicated by the higher critical angle  $\theta_{c1}$ . The inset shows the evolution of the layer thickness after different temperature treatments at the first heating step.

curve. At a concentration of 5.2 mol% a maximum remanent polarization of  $20 \mu\text{C cm}^{-2}$  appears which is significantly higher compared to the previous work.<sup>10</sup> Figure 6b) shows the comparison between three different deposition techniques for yttrium doped  $\text{HfO}_2$ . The CSD layers show a very similar concentration dependence compared to the

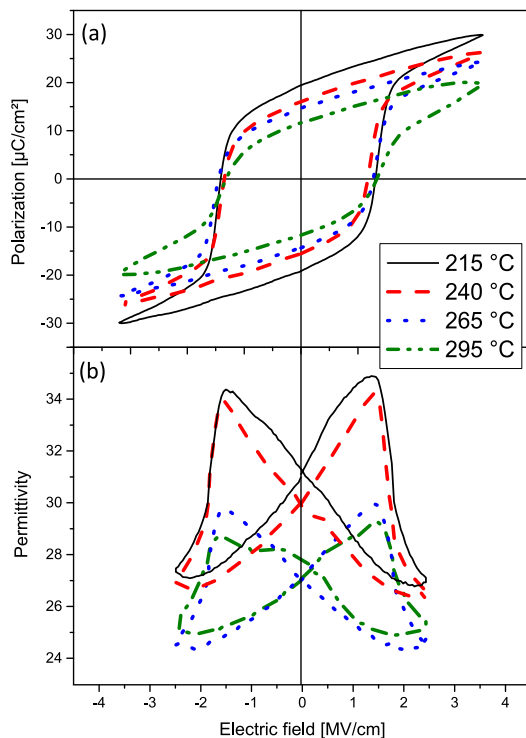


**Figure 4.** Influence of the temperature of the first heating step on the electrical properties after the final crystallization step at 800°C for a sample with 5.2 mol% yttrium doping (a): The remanent and maximum polarization decreases with rising temperature. The remanent polarization is decreased by 40% after a temperature increase of 80°C. (b): Similar to the polarization also the permittivity, which is calculated from capacitance measurements, decreases with rising temperatures.

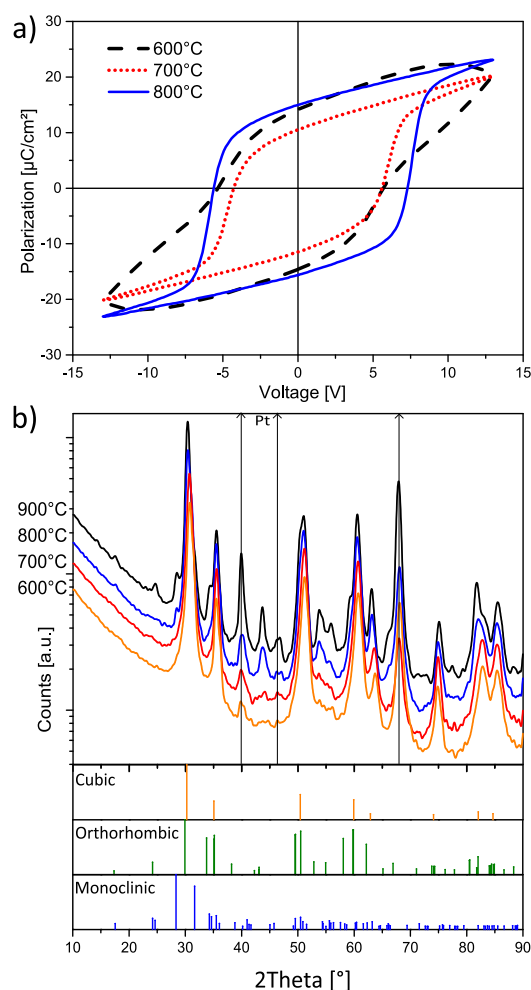


**Figure 5.** Influence of the crystallization temperature on the hysteresis and the corresponding crystal structure. The best ferroelectric hysteresis can be observed for 800°C. No electrical measurements for 900°C are given due to break down of the devices during wake-up.

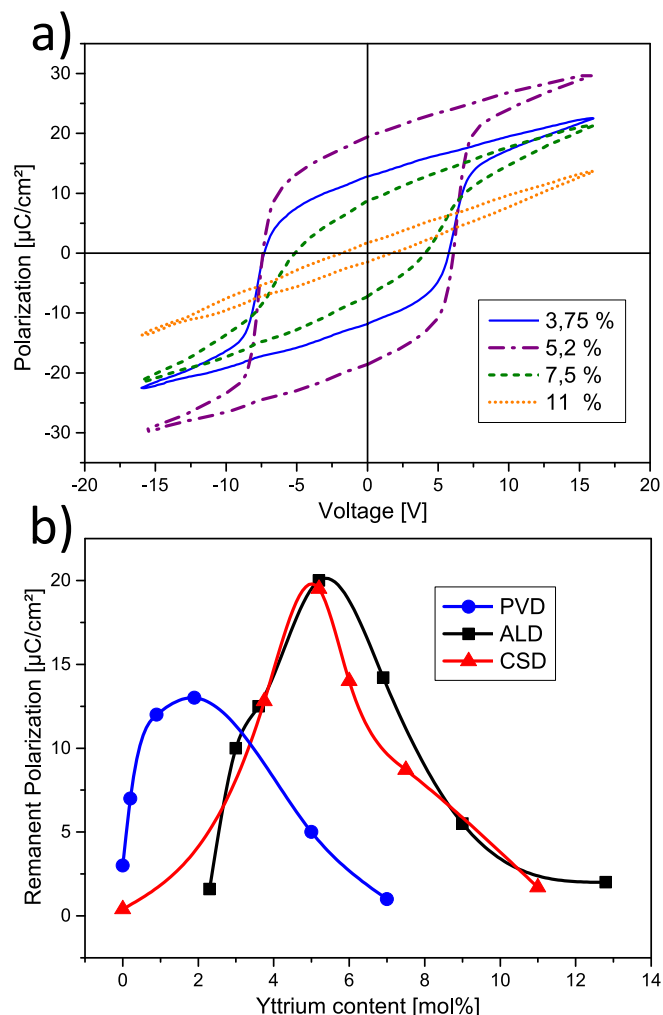


**Figure 6.** a): Dependence of the hysteresis on the yttrium concentration. b): Comparison of the CSD prepared samples with ALD (post deposition anneal)<sup>13</sup> and sputtering<sup>20</sup> concerning the remanent polarization as a function of the yttrium content.

ALD samples prepared with a post deposition anneal.<sup>13</sup> The layers prepared by sputtering show a similar behavior but the maximum of the remanent polarization is shifted to lower yttrium contents.<sup>20</sup> This could be explained by difference in the microstructure, or a different stoichiometry resulting from the deposition in reduced atmosphere. Figure 7 shows the hysteresis curves for different dopants from the lanthanide group which differ by their ionic radius.<sup>21</sup> No dependence of the ionic radius of the doping element on the ferroelectric hysteresis can be found as reported before.<sup>22</sup> This can be probably explained due to the small difference in the ionic radius from the smallest (Yttrium: 1.02 Å) to the largest (Lanthanum: 1.032 Å) ion.<sup>21</sup> From the results shown here it can be assumed that ferroelectricity in hafnium oxide films can be induced by doping with any element from the lanthanum series. Furthermore CSD deposition of ferroelectric films is highly suitable for further investigation of the influence of different dopants on the ferroelectric properties.

### Conclusions

In conclusion, we have demonstrated an optimized CSD routine for ferroelectric hafnium oxide films. It was proven that the heating steps have a strong influence on the formed layer and the ferroelectric properties. By an increase of the temperature of 90°C during the first heat-treatment the remanent polarization is reduced by 40%.

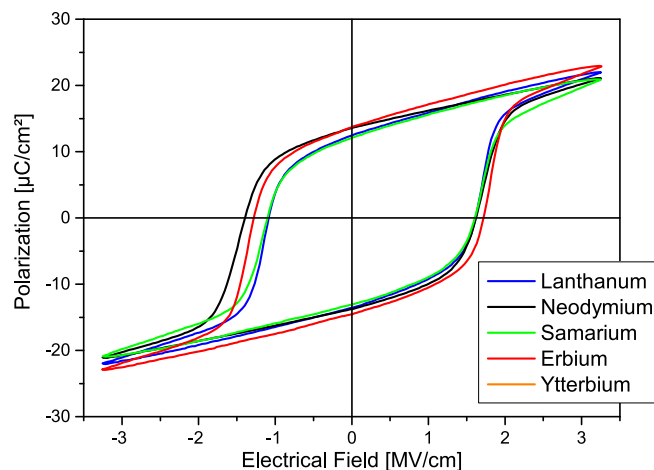


**Figure 7.** Dependence of the hysteresis curve on different dopants of the lanthanide group. A doping concentration of 5.2 mol% and a film thickness of approx. 42 nm are chosen for all dopants. An equal electrical field was applied to all samples.

The yttrium doped samples show similar characteristics concerning dopant concentration dependence and remanent polarization as ALD prepared samples and reach a maximum polarization of almost  $20 \mu\text{C cm}^{-2}$ . Ferroelectricity was also shown for doping with several elements from the lanthanide series.

Chemical solution deposition gives the opportunity of inexpensive, fast and flexible manufacturing of hafnium oxide based ferroelectrics for lead free piezoelectric und pyroelectric sensors and actuators and leads to a better understanding about the formation of the ferroelectric phase.

### Acknowledgments

This work was funded by German Research Foundation (Deutsche Forschungsgemeinschaft) within the scope of the project “Inferox” (project no. BO 1629/10-1).

### References

1. T. S. Boescke, J. Mueller, D. Braeuhaus, U. Schroeder, and U. Boettger, “Ferroelectricity in Hafnium Oxide thin films,” *Applied Physics Letters*, **99**, 102903 (2011).
2. S. Mueller, J. Mueller, U. Schroeder, and T. Mikolajick, “Reliability Characteristics of Ferroelectric Si: HfO<sub>2</sub> Thin Films for Memory Applications,” *IEEE Transactions on Device and Materials Reliability*, **13**, 93 (2013).
3. C. R. Bowen, J. Taylor, E. LeBoulbar, D. Zabeck, A. Chauhan, and R. Vaishe, “Pyroelectric materials and devices for energy harvesting applications,” *Energy & Environmental Science*, **7**, 3836 (2014).
4. Ya. Yang, Wenxi Guo, Ken C. Pradel, Guang Zhu, Yusheng Zhou, Yan Zhang, Youfan Hu, Long Lin, and Zhong Lin Wang, “Pyroelectric Nanogenerators for Harvesting Thermoelectric Energy,” *Nano Letters*, **12**, 2833 (2012).
5. Adnan Harb, “Energy harvesting: State-of-the-art,” *Renewable Energy*, **36**, 2641 (2011).
6. M. H. Park, H. J. Kim, Y. J. Kim, T. Moon, K. D. Kim, and C. S. Hwang, “Thin Hf<sub>0.95</sub>Zr<sub>0.05</sub>O<sub>2</sub> Films: A New Lead-Free System for Electrostatic Supercapacitors with Large Energy Storage Density and Robust Thermal Stability,” *Advanced Energy Materials*, **4**, 1400610/1- (2014).
7. Min Hyuk Park, Han Joon Kim, Yu Jin Kim, Taehwan Moon, Keum Do Kim, and Cheol Seong Hwang, “Toward a multifunctional monolithic device based on pyroelectricity and the electrocaloric effect of thin antiferroelectric Hf<sub>0.95</sub>Zr<sub>0.05</sub>O<sub>2</sub> films,” *Nano Energy*, **12**, 131 (2015).
8. M. H. Park, Y. H. Lee, H. J. Kim, Y. J. Kim, T. Moon, K. Do Kim, J. Mueller, A. Kersch, U. Schroeder, T. Mikolajick, and C. S. Hwang, “Ferroelectricity and Antiferroelectricity of Doped Thin HfO<sub>2</sub>-Based Films,” *Advanced Materials*, **27**, 1811 (2015).
9. Min Hyuk Park, Han Joon Kim, Yu Jin Kim, Taehwan Moon, and Cheol Seong Hwang, “The effects of crystallographic orientation and strain of thin Hf<sub>0.5</sub>Zr<sub>0.5</sub>O<sub>2</sub> film on its ferroelectricity,” *Applied Physics Letters*, **104**, 072901 (5 pp.)-07290 (2014).



10. S. Starschich, D. Griesche, T. Schneller, R. Waser, and U. Boettger, "Chemical solution deposition of ferroelectric yttrium-doped hafnium oxide films on platinum electrodes," *Applied Physics Letters*, **104**, 202903/1- (2014).
11. T. Schenk, S. Mueller, U. Schroeder, R. Materlik, A. Kersch, M. Popovici, C. Adelman, S. Van Elshocht, and T. Mikolajick, "Strontium Doped Hafnium Oxide Thin Films: Wide Process Window for Ferroelectric Memories," *ESSDERC* (2013).
12. J. Mueller, T. S. Boescke, U. Schroeder, S. Mueller, D. Braeuhaus, U. Boettger, L. Frey, and T. Mikolajick, "Ferroelectricity in Simple Binary  $\text{ZrO}_2$  and  $\text{HfO}_2$ ," *Nano Letters*, **12**, 4318 (2012).
13. J. Mueller, U. Schroeder, T. S. Boescke, I. Mueller, U. Boettger, L. Wilde, J. Sundqvist, M. Lemberger, P. Kuecher, T. Mikolajick, and L. Frey, "Ferroelectricity in yttrium-doped hafnium oxide," *Journal of Applied Physics*, **110**, 114113 (2011).
14. S. Mueller, C. Adelman, A. Singh, S. Van Elshocht, U. Schroeder, and T. Mikolajick, "Ferroelectricity in Gd-Doped  $\text{HfO}_2$  Thin Films," *ECS Journal of Solid State Science and Technology*, **1**, N123 (2012).
15. S. Mueller, J. Mueller, A. Singh, S. Riedel, J. Sundqvist, U. Schroeder, and T. Mikolajick, "Incipient Ferroelectricity in Al-Doped  $\text{HfO}_2$  Thin Films," *Advanced Functional Materials*, **22**, 2412 (2012).
16. Theodor Schneller, Rainer Waser, Marija Kosec, and David Payne, *Chemical Solution Deposition of Functional Oxide Thin Films*. Springer (2013).
17. S. Petit, S. Morlens, Z. Yu, D. Luneau, G. Pilet, J. Soubeyroux, and P. Odier, "Synthesis and thermal decomposition of a novel zirconium acetato-propionate cluster:  $[\text{Zr12}]$ ," *Solid State Sciences*, **13**, 665 (2011).
18. K. Knoth, R. Hühne, S. Oswald, L. Schultz, and B. Holzapfel, "Detailed investigations on  $\text{La}_2\text{Zr}_2\text{O}_7$  buffer layers for YBCO-coated conductors prepared by chemical solution deposition," *Acta Materialia*, **55**, 517 (2007).
19. M. Yu, N. Bovet, C. J. Satterley, S. Bengio, K. R. J. Lovelock, P. K. Milligan, R. G. Jones, D. P. Woodruff, and V. Dhanak, "True Nature of an Archetypal Self-Assembly System: Mobile Au-Thiolate Species on  $\text{Au}(111)$ ," *Physical Review Letters*, **97**, 166102-1-166102-4 (2006).
20. T. Olsen, U. Schroeder, S. Mueller, A. Krause, D. Martin, A. Singh, J. Mueller, M. Geidel, and T. Mikolajick, "Co-sputtering yttrium into hafnium oxide thin films to produce ferroelectric properties," *Applied Physics Letters*, **101**, 82905/1-4 (2012).
21. R. D. Shannon, "Revised effective ionic radii and systematic studies of interatomic distances in halides and chalcogenides," *Acta Crystallographica, Section A (Crystal Physics, Diffraction, Theoretical and General Crystallography)*, Denmark, **A32**, 751 (1976).
22. U. Schroeder, E. Yurchuk, J. Muller, D. Martin, T. Schenk, P. Polakowski, C. Adelman, M. I. Popovici, S. V. Kalinin, and T. Mikolajick, "Impact of different dopants on the switching properties of ferroelectric hafniumoxide," *Japanese Journal of Applied Physics*, **53**, 08LE02 (5 PP.)-08LE0 (2014).